Molecular Crystals and Liquid Crystals

Publication details, including instructions for authors and subscription information:
http://www.tandfonline.com/loi/gmcl20

Induced TGB phase in the (Nematic/Chiral Dopant) Liquid-Crystalline Composite System

Wen-Ren Chen [a] & Jenn-Chiu Hwang* [a]

[a] Department of Chemical Engineering and Materials Science, Neili, Taoyuan, R.O.C, Taiwan 320

Version of record first published: 02 Sep 2010

To cite this article: Wen-Ren Chen & Jenn-Chiu Hwang* (2004): Induced TGB phase in the (Nematic/Chiral Dopant) Liquid-Crystalline Composite System, Molecular Crystals and Liquid Crystals, 423:1, 85-96

To link to this article: http://dx.doi.org/10.1080/15421400490494535

Mol. Cryst. Liq. Cryst., Vol. 423, pp. 85–96, 2004

ISSN: 1542-1406 print/1563-5287 online
DOI: 10.1080/15421400490494535

Taylor & Francis
Taylor & Francis Group

INDUCED TGB PHASE IN THE (NEMATIC/CHIRAL DOPANT) LIQUID-CRYSTALLINE COMPOSITE SYSTEM

*Wen-Ren Chen and Jenn-Chiu Hwang**
Department of Chemical Engineering and Materials Science, Yuan-Ze University, Neili, Taoyuan, Taiwan 320, R.O.C.

In this study, an induced twist grain boundary (TGB) phase in the (nematic liquid crystal E7/chiral dopant S811) composite system has been investigated. The TGBA phase appeared in the range of E7/S811 = 75/25 ∼ 75/30 weight ratios. Different patterns in the TGBA* and SmA* phases were observed upon the untreated cells with different thicknesses. Optical microscopic texture like black coiled hoses and spiral fan-shaped pattern were observed in thinner and thicker cells separately. The transmittance experiments show that the thinner cells possess a higher transmittance, and it descended with increasing thickness. Cano-wedged cell method and selective reflectance method verified that the helical pitches decrease with the increase of the chiral dopant concentration. The shift in the highest reflectance and the corresponding wavelengths occurred as the thickness increased: the former shifts to lower one and the latter shifts to higher one.*

Keywords: twist grain boundary phase; selective reflectance; helical pitch

INTRODUCTION

Twist grain boundary (TGB) phase is a frustrated phase first predicted by Renn and Lubensky [1]. It was normally found between cholesteric phase and smectic A/smectic C phase. The first report about observing the TGB phase was announced by Goodby *et al.* in 1989 [2]. Before that, the hypothesis that the action of chirality to the liquid crystalline molecules in the N* phase is analogous with an external magnetic field acting on the normal metal conductor was proposed by de Gennes [3]. The former causes a transition from cholesteric to SmA phase and the later a transition from normal conductor to type II superconductor. The normal proposed TGB orientation structure is characterized by a helical superstructure, smectic slabs, and the

*Corresponding author. E-mail: cejhwang@saturn.yzu.edu.tw

helical axis parallel to the smectic slabs. It was proposed that the adjacent two slabs would be separated by the parallel and helical dislocation lines, and the optical microscopic filament-like textures were observed in the confined geometry of liquid crystal cell without rubbing treatment [4].

Many ferroelectric and cholesteric liquid crystals with high chirality were synthesized so that the TGB phase was observed in a homologous series [2,4–8]. The TGB phases came into public notice in the binary mixture constructed from a ferroelectric liquid crystal and a chiral dopant [9] or ternary mixture from two nematic liquid crystals and a cholesteric liquid crystal [10]. Recently R Dhar and coworkers reported about a (nematic liquid crystal/cholesteric liquid crystal) mixture that induced a TGB phase in some molar ratios [11,12]. Also, some binary mixtures from a smectic mesogen and a cholesteric mesogen or a chiral dopant that induce the TGB phase were reported [13]. It was noticed that most of the mentioned multicomponent mixtures included at least a ferroelectric or cholesteric liquid crystal. It's why we try a binary composite system constructed from nematic liquid crystal and chiral dopant (without liquid crystalline mesophase), and look forward to inducing a frustrated phase.

In this study, we mixed a nematic liquid crystal E7 with a chiral dopant S811 to discuss the phase behavior of the binary composite. The differences in the optical microscopic textures of the TGB phase and the transmittance of the cell among different cell thicknesses were investigated. Both the Cano-cell method and selective reflectance method were employed to measure the helical pitch. The thickness dependence of the reflectance of the cells was also studied.

EXPERIMENTAL

Figure 1 is the phase transition temperature of the experimental materials. Both the nematic liquid crystal E7 and chiral dopant S811 were purchased from Merck Co., (Tokyo, Japan) and no further purification process was executed. The nematic liquid crystal/chiral dopant mixture was first dissolved in solvent, and the composite was prepared by solvent casting. The above sample was injected into the sandwiched cell constructed from two transparent ITO glasses and 4 100 μm PET spacers in the liquid crystalline phase. All the cells were made without any treatment upon the ITO glasses.

The phase transition behavior and the aggregation states of the E7/S811 composite were investigated by differential scanning calorimeter (DSC: Perkin-Elmer DSC-7) and polarized optical microscopy (POM: Nikon FXA) equipped with a hot stage (Mettler FP82 and FP90). The heating or cooling cycle rate of DSC is 5°C per minute and the cooling rate is 0.1–3°C per minute upon the POM observation of phase transition.

(1) Nematic liquid crystal: E7

K - -10℃ - N - 60℃ - I

(2) Chiral dopant: S811

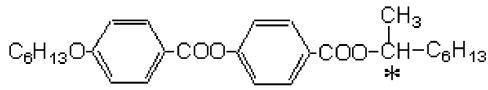

K - 47.8℃ - I

FIGURE 1 The phase transition temperature of the nematic liquid E7 and chiral dopant S811.

Helical pitches of binary composite were measured by Cano cell [14]. The glass substrates were 10 mm in width and 15 mm in length, and the spacer inserted between two parallel-rubbed glasses was 25 μm thick. The Grandjean-Cano dislocation lines were observed by the POM with hot stage. He-Ne laser with wavelength 632.8 nm was used as the light source to measure the transmittance change of the cell without any polarizer. The scattering light by the cell was detected by a photodiode and recorded by a digital storage oscilloscope. The distance between the cell and photodiode was about 30 cm. Hitachi U4100 UV-VIS-NIR spectrometer was employed to measure the reflectance of the cell filled with the binary composite.

RESULTS AND DISCUSSION

The Phase Behavior and Aggregation States of the Binary Composite

E7 is a liquid crystalline mixture with broad nematic phase, and S811 is a chiral dopant without any liquid crystalline phase. Several induced liquid-crystalline mesophases were observed in the mixtures of E7 and S811 at different weight ratios [15]. Among them, induced smectic phase was found in the weight region of 55/45 to 20/80. It coincides with the result that a smectic phase was induced by mixing nematic cyanobiphenyl and benzoate compounds [16,17]. Upon observation of the untreated cell, it was noticed that the E7/S811 composites in the weight ratio of 75/25–70/30 exhibited a sequence of the mesophases:

Iso (41.3°C) BP III (39°C) BP I or II (36.3°C) N* (23.1°C) TGBA* (22.6°C) SmA*
Iso (39.5°C) BP III (37.2°C) BP I or II (32.1°C) N* (25.9°C) TGBA* (24.8°C) SmA*

Here we used an asterisk (*) to denote all liquid crystal phases consisting of chiral structure [18]. The former (75/25 sample) and the latter (70/30 sample) were observed in a 12 μm untreated cell, and the cooling rate was 1.2°C per minute. It interested us that the smectic phase in this phase series had a spiral fan-shaped texture. That means the helical superstructure is kept during the cooling process from TGBA* phase to SmA* phase. When consecutively decreasing the temperature to near 0°C, the same pattern was still observed under polarized POM. We also noticed that this spiral texture in the thinner cell was different from that in the thicker cell. Figure 2 shows the microscopic photographs of the 70/30 composites in the cells with thickness 4 μm and 20 μm during the cooling process. Optical texture in the TGBA* phase of 4 μm cell was apparently the filament-like pattern as shown Figure 2(a). The filament around the central core gradually disappeared with decreasing temperature. After all the filament disappeared, the TGBA* phase changed to SmA phase with a texture that resembled many black coiled hoses (Figure 2(b)). As Figure 2(c) shows, the optical texture in the TGB phase of 20 μm cell was like the eddy of water in a washing machine. Further cooling the TGBA* phase also changed to SmA phase, but the observed texture was like a helical fan-shaped pattern. It was also noticed that the spiral pattern would be affected by the cooling rate. The slower cooling rate would induce the more complete spiral-like pattern.

The thinner cell is likely to offer not enough space to aggregate the molecule blocks constructed from several smectic layers to fanlike or focalconic shape, so the director of molecule orients spirally in a plane parallel to the substrate. Figure 3 shows the representative scheme: Figure 3(a) and 3(b) are for the thinner cell, and 3(c) and 3(d) are for the thicker cell. The superstructure in spiral fashion is proposed from the top view of the thinner cell as in Figure 3(a). The layer planes (normal to the director of the smectic molecules) are parallel to each other in the smectic slabs. The angles α between any two adjacent slabs are the same, and the layer plane in the slab will parallel the one in the first block after rotating 2π angles. By this fashion, the molecules orient as a spiral structure on the top view. The smectic layer planes are almost perpendicular to the substrate from the side view of the cell in Figure 3(b), and the directors of the molecules orient towards the substrate plane as a screw orientation. The space between two substrates was comparatively tiny so that the molecules orient parallel to the substrate. This layer-stacking structure will induced a dark hoselike pattern since the observation is under the cross polarization. The top view of the thicker cell, as Figure 3(c) shows, was almost the same with Figure 3(a). The layer plane of upper block was a little inclined with the lower one, but the layer planes also parallel each other in a block. Figure 3(d) shows the side view of the thicker cell; the molecule

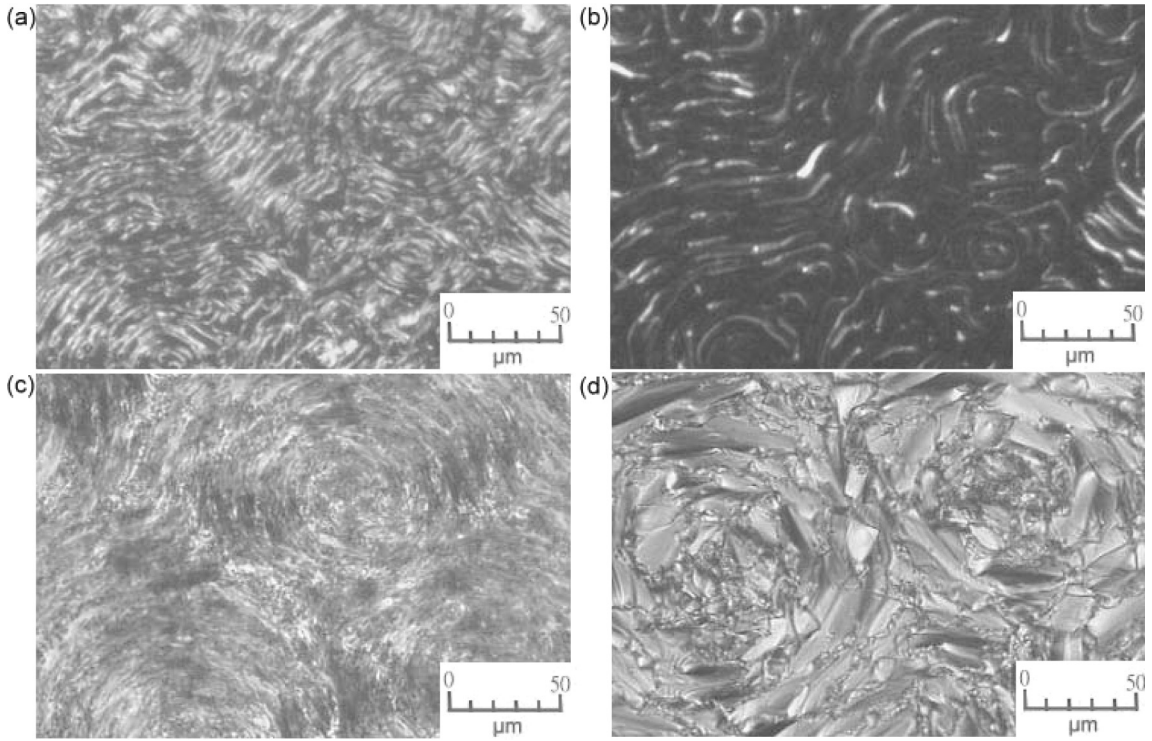

FIGURE 2 The optical microscopic texture photographs of E7/S811 = 70/30 sample in different thicknesses of the cell were shown: (a) TGBA* phase, T = 25.7°C, 4 μm; (b) SmA phase, T = 23.7°C, 4 μm; (c) TGBA* phase, T = 24.7°C, 20 μm; and (d) SmA phase, T = 21°C, 20 μm. (See COLOR PLATE III).

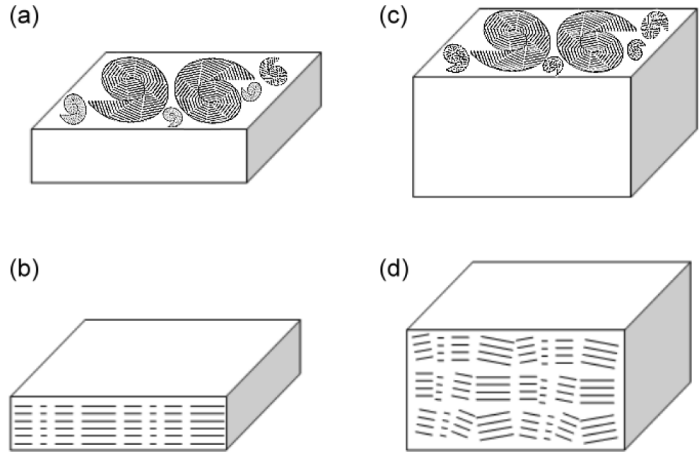

FIGURE 3 The schematic illustrations of the thickness effect on the binary composite were drawn. (a) top view and (b)side view of thinner cell and (c) top view and (d) side view of thicker cell.

directors are parallel to each other in every slab but slant in different slabs. This layer-stacking structure will induce birefringent fan-shaped pattern under the cross polarization. It was also noticed that the phase transition temperature (TGBA* → SmA*) shifts to lower value from the thinner cell (4 μm) to the thicker cell (20 μm). It is possible that more uniform distribution of the temperature in the thinner cell contributes to the phase transition during the cooling process.

Figure 4 shows the temperature dependence of the transmittance in the untreated 12 μm cell filled with the 70/30 sample. Figures 4(a) and 4(b) are for the cooling and heating process, respectively, and the cooling or heating rate is 1.2°C per minute. The photo-current signal is about 20 mV a scale in the vertical axis, and the recording time is 50 s a scale in the horizontal axis. The transmittance of the empty cell is as the reference (100%), and the dark state is underground connection (0%). As Figure 4(a) shows, as the transmittance decreased from highest value at about 39.6°C, it corresponded to the isotropic liquid-blue phase transition. From 39.6 to 32.2°C it was found that the transmittance decreases slowly to about 82%, and two flat regions were observed. Compared with the observation under cross-polarized POM, it is likely that BPIII and BPI or BPII appeared in these two flat regions. The transmittance sharply descended from 82% on further cooling, and it reached the lowest value (about 27%) at 30.6°C and ascended slowly to about 56% at 26.2°C. This sharp change of transmittance corresponded to the chiral nematic phase, and the phase range is from 32.2 to 26.2°C. The spiral lines were observed at

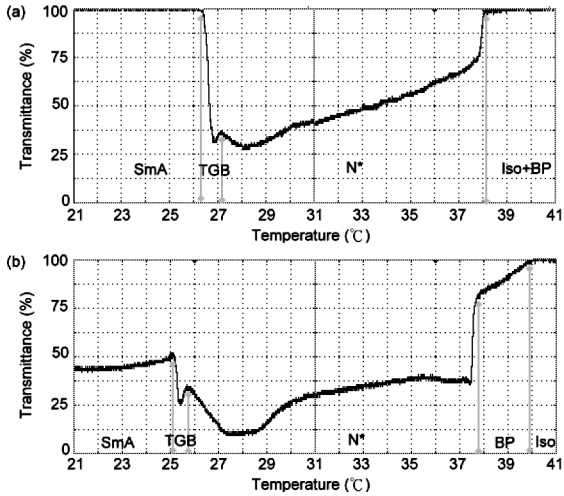

FIGURE 4 The transmittances of the binary composite (70/30, 12 μm) were shown on the cooling and heating process.

about 26.1°C under the observation of cross-polarized POM, and it meant that the N* to TGBA* phase appeared at this temperature. From the change of transmittance, the same phase transition occurred at about 26.2°C. The transmittance decreased and increased abruptly during 1.6°C range, and it corresponded to the TGBA* phase. The orientation of the molecules reoriented as a spiral fashion in the TGBA* phase and caused the transmittance to decrease suddenly to another lower value. Following the completion of the spiral orientation, the transmittance rose again and the phase transferred to the smectic phase. This sharper change of transmittance on the TGBA*–SmA* region is caused by the formation of spiral lines. On subsequent cooling, the transmittance was kept at the constant value (67%) until 21°C or lower. Figure 4(b) shows the change of transmittance on the heating process. The corresponding phase transitions are SmA–TGBA*, TGBA*–N*, N*–BP, and BP–Iso phase, and the transition temperatures are 24.8, 25.6, 37.1, and 39.2°C, respectively. The lowest transmittance (31%) appeared at about 28°C, and it belongs to N* phase with planar structure. From tracing change of transmittance on the heating or cooling process, the phase transition states are apparently verified.

In order to study the effect of thickness on the transmittance, three cells with different thicknesses were used to compare the difference during the cooling process, as Figure 5 shows. Figures 5(a) and 5(b) were recorded from 4 and 20 μm cells, respectively. It was found that the transmittance descended with increasing thickness despite which liquid crystalline phase.

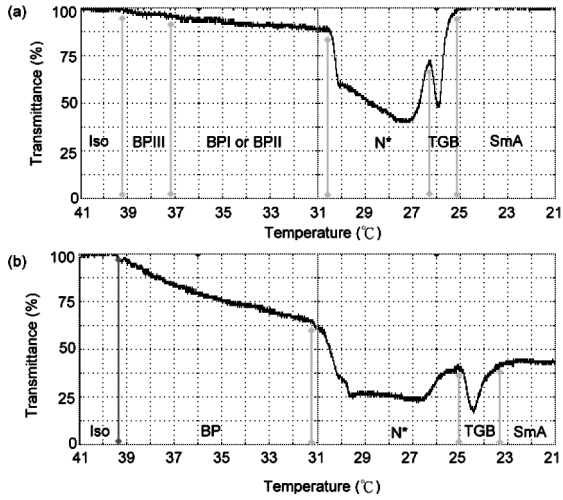

FIGURE 5 The transmittances of the 70/30 samples were detected on the cooling process, (a) for 4 μm cell and (b) for the 20 μm cell.

The phase transitions of two cells were both the same with the 12 μm, but the phase transition temperatures were a little different. As Figure 5(a) shows, the blue phase range was from 39.2 to 30.6°C and is a flat region (about 37.2°C) separated into two types, where one is BP III and the other is BPI or BPII. However, it is difficult to classify the blue phases from the thicker cell as Figure 5(b). The transmittance of the cell (N* phase range) decreased with the temperature on the thinner cell but remained at the same level on the thicker cell. It is possible that the thinner cell was easily affected by the thermal disturbance.

Figure 6 is the transmittance diagram of two cells on the heating process. The phase transitions determined by this diagram were SmA → TGBA* → N* → BP → Iso following the increase of temperature. The same result, that the thinner cell possesses higher transmittance than the thicker cell regardless of phase, was derived as compared with Figure 5. It was found that the transmittance of the TGBA* phase descended and ascended suddenly during 1°C and descended again in the N* phase. The transmittance of two cells increased gradually with the temperature in the N* region. On further heating, the transmittance rose to the highest value at about 37–38°C. From the Figure 6(a) it was difficult to distinguish the blue phase from the isotropic phase. The blue phase of the thicker cell was apparently verified between the N* and Iso phase, as shown in Figure 6(b).

Cano wedge-cell method was usually used to measure the helical pitch of the liquid crystalline sample. Figure 7 shows the Grandjean-like textures of

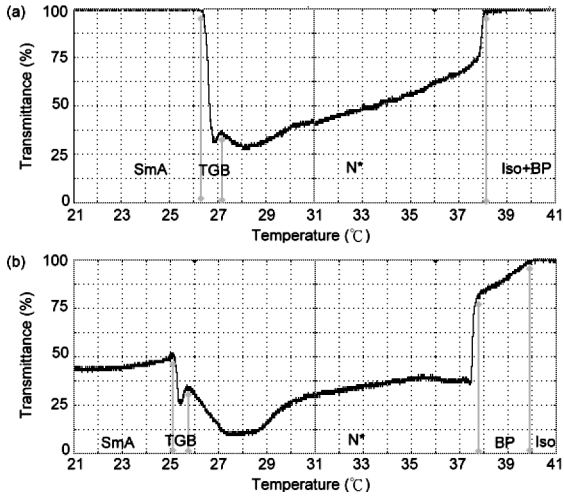

FIGURE 6 The transmittances of the 70/30 samples were detected on the heating process, (a) for 4 μm cell and (b) for the 20 μm cell.

the E7/S811 mixture under the observation of the Cano-cell. Figures 7(a) and 7(b) were measured as the 70/30 and 75/25 cells with homogeneous alignment. The distance between two Grandjean lines is proportional to the half of helical pitch. With the help of objective microscope micrometer

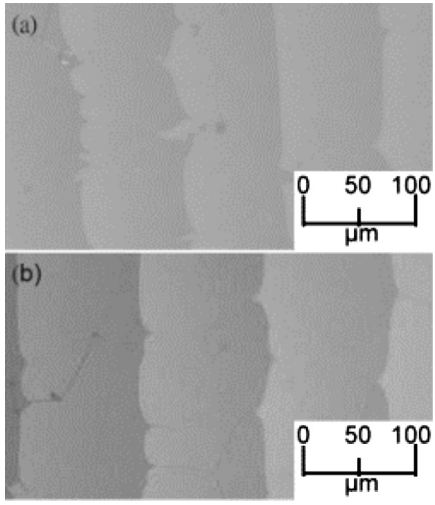

FIGURE 7 The Gradjean-Cano texture photographs of the binary composites were pictured on (a) 70/30 and (b) 75/25 samples.

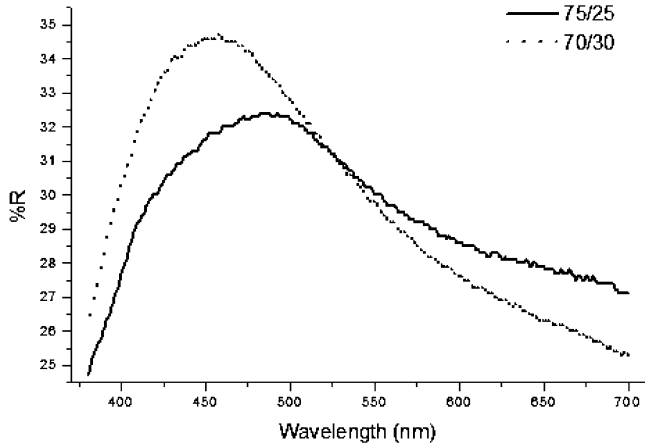

FIGURE 8 The reflectance spectra of the binary composites were overlapped as 70/30 and 75/25 samples.

(100 scales within 1 mm), the average distances of two samples were measured as 90 and 105 μm. The relative pitches calculated were 380 and 440 nm, respectively. The helical pitches decreased with the increase of the chiral dopant concentration.

The measurement of the reflectance was another technique to calculate the helical pitches. Figure 8 is the overlapping reflectance spectra of 70/30 and 75/25 samples. The samples were prepared by cooling down to about 30°C from the isotropic liquid and were measured from the 400 to 700 nm. As Figure 8 shows, the corresponding wavelengths to highest reflectance were about 460 and 490 nm. From the formula below, the helical pitches calculated were about 310 and 330 nm ($n_{avg} \doteqdot 1.5$):

$$\lambda_0 = n_{avg} \times P.$$

The difference of helical pitches was found between two measurements. It is possible that the average refractive index is smaller than 1.5 and experimental error. The trend that the helical pitches decrease with the increase of the chiral dopant concentration is nevertheless the same during the two methods. This result coincides with a previous report by Kramarenko and coworkers [19].

The overlapping reflectance-spectra of three cells filled with the same sample 70/30 at different thickness 4, 20, and 100 μm is shown in Figure 9. From this diagram, the wavelengths to achieve the highest reflectance of three samples were all observed at about 450–550 nm. It was noticed that the corresponding wavelength shifts to a higher one with increasing cell thickness. In addition, the highest reflectance also decreased with the

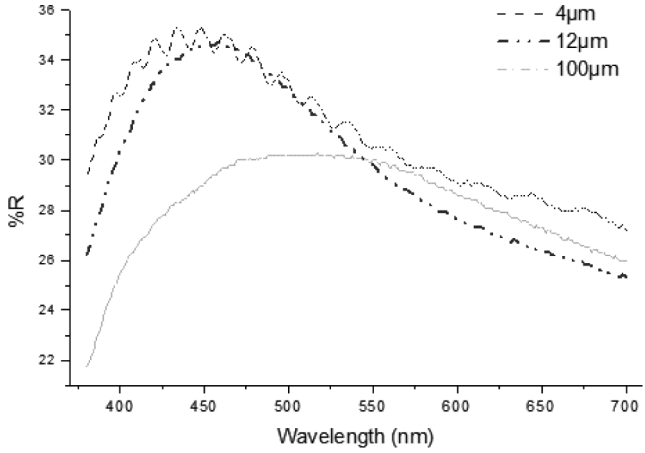

FIGURE 9 The reflectance spectra of the 70/30 samples were recorded in different cell thicknesses—4, 12, and 100 μm.

increase of the cell thickness. It is likely that the larger spaces are supplied in a thicker cell, and the molecules orient as a more disordered trend. That means more light radiations scatter and reflect repeatedly inside the cell and cause the highest reflectance to decrease and the corresponding wavelength to shift.

When the addition of chiral dopant was tiny, the N* phase with fingerprint or focal-conic texture was induced. Nevertheless, the addition was larger and would induce fan-shaped SmA phase [14]. The content of chiral dopant between these two extremes will induce two frustrated BP or TGBA* phases. This result is similar to the studies of R Dhar *et al.* [11,12]. That means rodlike molecules with a chiral terminal, regardless of cholesteric liquid crystal or nonliquid-crystalline compound, could mix with a nematic mesogen to induce the BP and TGB phases.

CONCLUSIONS

We reported that the twisted grain boundary phase was induced in the special ratios of the binary composite system constructed from a nematic liquid crystal E7 with a chiral dopant S811. Optical microscopic texture like black coiled hoses and spiral fan-shaped pattern were observed in the thinner and thicker cells respectively. The transmittance experiments show that the thinner cell possesses a higher transmittance, and it descended with increasing thickness. Cano-wedged cell method and selective reflectance method verified that the helical pitches decrease with the increase

of the chiral dopant concentration. The shift in the highest reflectance and the corresponding wavelengths occurred with increase of the thickness: the former shifts to lower one and the latter shift to higher one.

REFERENCE

[1] Renn, S. R. & Lubensky, T. C. (1988). *Phys. Rev. A, 38*, 2132–2147.
[2] Goodby, J. W., Waugh, M. A., Stein, S. M., Chin, E., Pindak, R., & Patel, J. S. (1989). *Nature, 337*, 449–452.
[3] de Gennes, P. G. (1972). *Solid State Commun., 10*, 753–756.
[4] Goodby, J. W., Waugh, M. A., Stein, S. M., Chin, E., Pindak, R., & Patel, J. S. (1989). *J. Am. Chem. SOC., 111*, 8119–8125.
[5] Dierking, I., Gieβelmann, F., & Zugenmaier, P. (1994). *Liq. Cryst., 17*, 17–22.
[6] Li, M. H., Laux, V., Nguyen, H. T., Sigaud, G., Barois, P., & Isaert, N. (1997). *Liq. Cryst., 23*, 389–408.
[7] Wu, S. L., Yen, P. C., & Hsieh, W. J. (1998). *Liq. Cryst., 24*, 741–746.
[8] Cha, S. W., Jin, J. I., Achard, M. F., & Hardouin, F. (2002). *Liq. Cryst., 29*, 755–763.
[9] Dierking, I. (2001). *Liq. Cryst., 28*, 165–170.
[10] Hwang, J. C., Liang S. C., & Liang, K. H. (1998). *Jpn. J. Appl. Phys., 37*, 4444–4447.
[11] Dhar, R., Pandey, M. B., & Agrawal, V. K. (2003). *Phase Trans., 76*, 763–780.
[12] Dhar, R., Agrawal, V. K., & Pandey, M. B. (2003). *Phase Trans., 76*, 959–974.
[13] Kramarenko, N. L., Kulishovs, V. I., Kutulya, L. A., Semenkova, G. P., Seminozhenko, V. P., & Shkolnikova, N. I. (1997). *Liq. Cryst., 22*, 535–541.
[14] Cano, R. (1968). *Bull. Soc. Fr. Mineral. Cristallogr., 91*, 20–28.
[15] Chen, W. R. & Hwang, J. C. *Liq. Cryst.,* accepted July 25, 2004, in press.
[16] Engelen, B., Heppke, G., Hopf, R., & Schneider, F. (1978). *Ann. Phys., 3*, 403–410.
[17] Domon, M. & Billard, J. (1979). *J. Phys.* (*Paris*)*, 40*, C3–413–416.
[18] Dierking, I. & Lagerwall, S. T. (1999). *Liq. Cryst., 26*, 83–95.
[19] Kramarenko, N. L., Semenkova, G. P., Kulishovs, V. I., Tolochko, A. S., Kutulya, L. A., Vaschenko, V. V., & Handrimajlova, T. V. (1994). *Liq. Cryst., 17*, 351–357.